42nd AIAA/ASME/SAE/ASEE Joint Propulsion Conference & Exhibit
9 - 12 July 2006, Sacramento, California

AIAA 2006-4655

Numerical simulations of a 2kW Hall thruster

E. Ahedo, * I. Maqueda, † and A. Antón ‡
Universidad Politécnica de Madrid, Spain
Y. Raitses, N. J. Fisch
Princeton Plasma Physics Laboratory

Simulations of the 2kW Hall thruster of the Princeton Plasma Physics Laboratory are carried out with the two-dimensional hybrid code HPHall-2. The different aspects of the plasma response and thruster performances are discussed. A preliminary comparison with experimental data is presented. There is a reasonable agreement in basic aspects of the plasma response but improvements or adjustments in the modelling of some phenomena are needed.

I. Introduction

This work reports first results on the numerical simulation of the 2kW Hall thruster of the Princeton Plasma Physics Laboratory(PPPL) with the code HPHall-2. Both the PPPL thruster and the code HPHall-2 have been extensively described in several papers .[1–4] The main goals of this cooperative project are: 1) the comparison of experimental and simulation results; 2) a better comprehension of the plasma physics in Hall thrusters; and 3) the identification of those aspects of the physical and numerical modelling that require revision or improvement. Special attention is going to be paid to electron-wall phenomena and the electron energy balance, which are subjects of high interest to the two research groups. The results presented here correspond to the first successful simulations and there has been almost no time for a methodic comparison with experimental data.

II. Simulation results

Figure 1 (a) shows a sketch of the simulation domain, the magnetic lines (which define the integration mesh for the electron equations) and the simulation mesh for the heavy particles subcode of HPHall-2.

The two-dimensional (2D) macroscopic equations for electrons are reduced to one-dimensional (1D) equations on the variable λ defining the magnetic streamlines. These 1D equations include source terms for the fluxes of electron mass, momentum, and energy from/to the thruster walls. These source terms are provided by a subcode solving the appropriate Debye sheath model. Integration on λ proceeds from the external boundary of the domain to the separatrix S, shown in Fig. 1. The separatrix is the line separating streamlines that intersect the anode from those that they do not. The integration of electron equations in the near-anode region SB, from S to the anode sheath edge B, has been improved recently and is reported in another paper.[5] The large extension of this near-anode region in the present case ($\sim 35\%$ of the channel meridian area) has posed a serious convergence challenge for the electron numerical scheme. The external boundary coincides with the neutralization surface, where the inwards electron current is delivered at a temperature

*Professor, Escuela Técnica Superior de Ingenieros Aeronáuticos(ETSIA), eduardo.ahedo@upm.es, AIAA Member.
†Student, ETSIA.
‡Student, ETSIA.

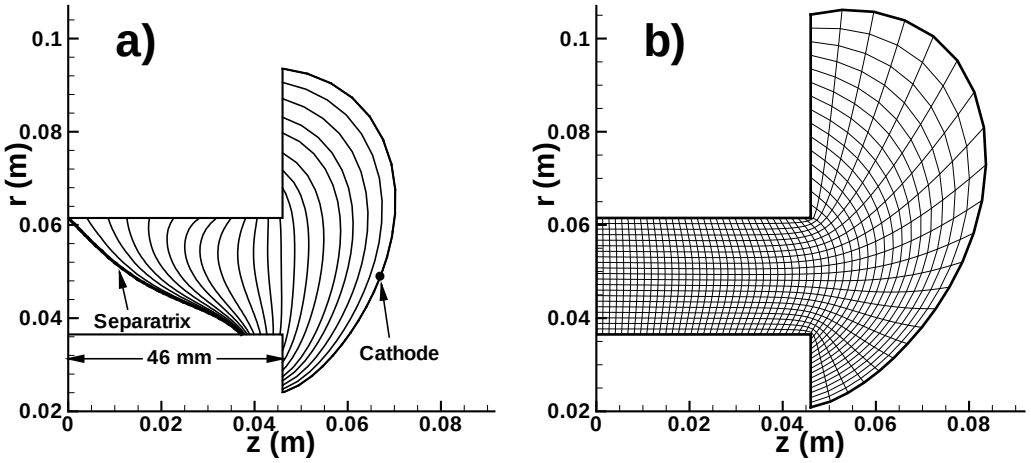

Figure 1. (a) Schematic of the PPPL 2kW thruster chamber and magnetic lines. Electrons are inserted into the plasma plume at the magnetic line crossing point C, where the cathode potential reference is placed. The mesh of magnetic lines (35 nodes) is the one used by the electron subcode. (b) Simulation mesh for the particle subcode (50x22 cells); $\sim 30.000 - 40.000$ particles per species are used.

of 5eV for most of the simulations here. The cathode reference potential is placed at point C in the neutralization surface.

The electron-wall interaction at the lateral Boron Nitride(BN) walls depends strongly on the secondary-electron emission(SEE) of the material. With respect to the external walls of the thruster, the inner one is recovered by BN, but the outer one is metallic. However, the present simulations consider that all walls are recovered by BN. The BN compound of the PPPL thruster yields 100% SEE for an electron energy $E_1 \sim 35 - 40$eV.[6] For the simulations presented here we have considered a simple SEE yield model consisting of cold true-secondary emission, no reflected electrons, and an 80% thermalization of the electron distribution function. This partial thermalization increases the electron temperature for the sheath charge-saturation limit (CSL) from $T_e^* \sim 21 - 24$eV (at total thermalization) to $T_e^* \sim 26 - 30$eV.[7,8] The plasma-wall subcode of HPHall-2 gives the plasma flux recombined at the walls, the ion and electron energies deposited at the walls, and the wall-induced electron transport caused by secondary/primary exchanges (i.e. wall-collisionality). The state of neutrals created from wall recombination depends on the ion energy accommodation;[3] a factor $a_w = 80\%$ has been used here, which means that neutrals from wall recombination are injected with $\sim 20\%$ of the ion impact energy.[3]

A. Two-dimensional maps

The reference case for the simulations is $\dot{m}_A \simeq 4.8$ mg/s (anode mass flow) and $V_d = 300$V (discharge voltage, between C and anode). The maximum radial magnetic field is around 173 G. HPHall-2 includes an empirical parameter α_{ano} accounting for turbulent (i.e. Bohm-like) diffusion caused by correlated azimuthal fluctuations of plasma density and electric field.[9,10] A relative fluctuation level of $\alpha_{ano} = 1\%$ was selected. Figure 2 presents two-dimensional maps of main plasma magnitudes. The maximum ionization rate is reached in the region of maximum plasma density. The main acceleration zone (characterized by the drop of the plasma voltage) is downstream of the ionization region. The voltage drop in the acceleration region is 80-90% of V_d, in agreement with experimental results.[2] There is also a basic agreement in the T_e profile, which presents a maximum in the acceleration region.[2] In the electron advance from cathode to anode, Joule heating starts increasing the electron temperature, then T_e decreases because of

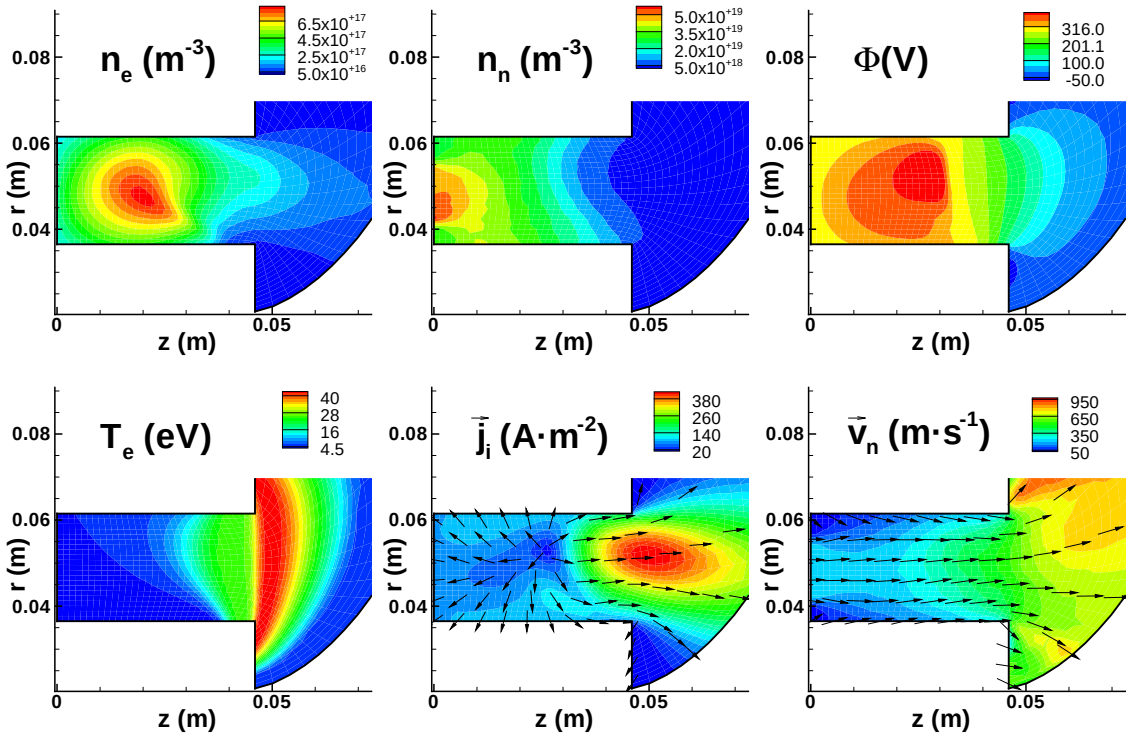

Figure 2. Plasma response for $\dot{m}_A \simeq$=4.8 mg/s and $V_d = 300$V. Vectors for the neutral velocity and the ion current density mark only the magnitude direction. $en_e\boldsymbol{v}_i$, and $\boldsymbol{u}_n$. Plume region is shown partially.

losses at lateral walls (in the thruster exit vicinity mainly) and then ionization (in a deeper region of the channel). The lines T_e = const coincide with the magnetic streamlines. The asymmetry of the magnetic topology with respect to the channel median makes asymmetric the plasma density map. The effect is less pronounced on the electric potential map because of the small electric field inwards of the acceleration region.

Figure 3 illustrates the relative location of magnetic streamlines and equipotentials and the effect of these last ones on the ion flux. We observe first that equipotentials do not follow closely the streamlines; it remains to be investigated how changes in the magnetic field curvature modify the equipotentials. On the other hand we observe that ion current is well adapted to the potentials gradients.

B. Plasma interaction with lateral walls and anode

The sheath subcode yields detailed results of the plasma-wall interaction parameters. The equations for the (electron-repelling) sheath dictate that for a stationary sheath solution to exist ions must enter the sheath sonic or supersonically, which is known as the Bohm condition. Although the exact expression of this condition is not simple due to the complex electron/ion distribution functions, $M_i \equiv v_{iN}/\sqrt{T_e/m_i} = 1$ is a good enough approximation (subscript N refers to the component perpendicular to the wall). Plasma density and ion velocity at the quasineutral plasma boundary (i.e the sheath edge) are very sensitive to the weighting algorithm used by the PICMCC subcode, and radial plasma profiles tend to be underdeveloped if the mesh is not thin enough.[4,11] Figure 4 shows the ion Mach number in the present simulations with the corrected-weighting(CW) algorithm (the alternative, more intrusive, Bohm-forcing algorithm was rejected since it perturbed convergence).

The differences between the profiles at the inner and outer walls are due to the asymmetry

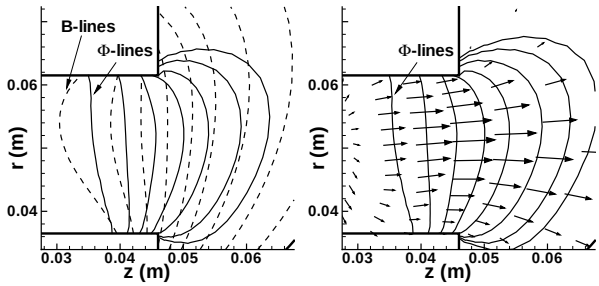

Figure 3. Magnetic streamlines, equipotentials, and ion density current vectors (scaling with vector magnitude) near the thruster exit, for the case of Fig.2.

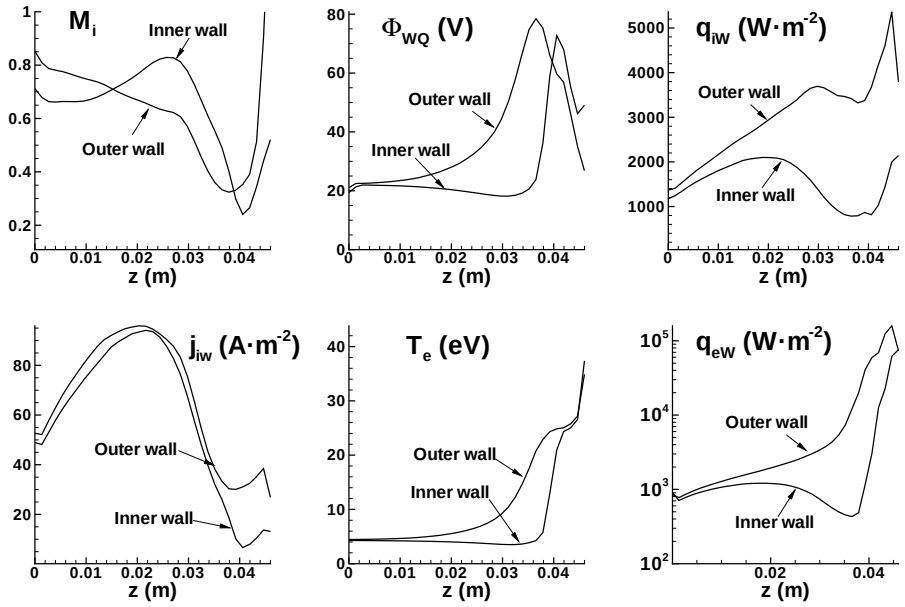

Figure 4. Plasma interaction with lateral walls for the case of Fig.2. M_i is ion Mach number (based on perpendicular velocity) at the lateral contours of the quasineutral domain. ϕ_{WQ} is the sheath potential fall, j_{iW} is the ion/electron density flux to the walls. q_{iW} and q_{eW} are energy fluxes to the walls (not to the sheaths) of ions and electrons.

of the magnetic field. The separatrix S intersects the inner and outer walls at $z \sim 36$ mm and $z = 0$ respectively(Fig.1). Since electron temperature is constant at magnetic streamlines, and $T_e \sim 5$eV at the separatrix (Fig.2), the 'near-anode' region BS is rather cold. This explains that T_e is smaller at the inner wall, leading to smaller potential falls ϕ_{WQ} and energy losses q_{eW} there (Fig.4). The ion current to the wall, j_{iW} (Fig.4), depends on the plasma density(Fig.2), which is governed by the 2D dynamics in the bulk of the plasma.

Sheaths are charge saturated only in thin regions near the thruster exit (where $T_e > 26$eV, roughly). For a charge saturated sheath the counterstreaming fluxes of primary and secondary electrons are $\sim 80-100$ times larger than the ion flux (j_{iW}) and their difference is exactly the ion flux. This explains the enormous electron energy flux (q_{eW}) near the thruster exit. Notice that ϕ_{WQ} increases with T_e but decreases with the SEE yield, which explains the peaks of ϕ_{WQ} near the thruster exit. The ion energy flux to the wall q_{iW} is the product of the ion flux and the mean energy per impacting ion, which includes the energy gained by ions when crossing the sheath.

The metallic anode occupies the whole rear surface. Figure 5 shows 2D maps of the region close to the anode, and the potential profile in the anode sheath, ϕ_{AB}. The anode sheath is negative

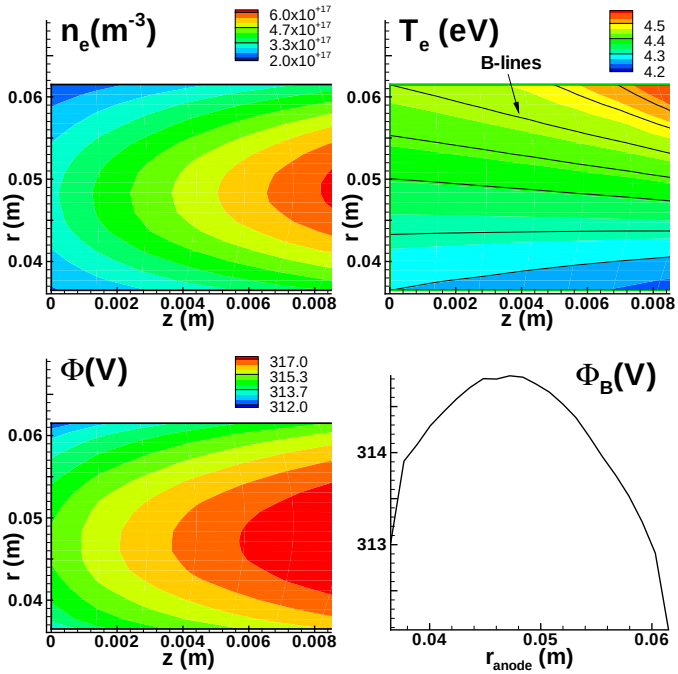

Figure 5. Plasma interaction with the anode and near-anode region for the case of Fig.2. The anode potential is $\phi_A = 300$V.

(i.e. electron repelling) which is consistent with a large ion backstreaming region. Dorf et al.[12] have reported experimental results of both positive and negative sheaths; we expect to analyze this kind of transitions in the future.

C. Evolution with the discharge voltage

Figure 6 presents the evolution of thruster performances when the discharge voltage is varied from 110V to 600V, keeping constant the magnetic field (as in Ref. 2) and the mass flow. Figure 7 complements Fig. 6 by comparing plasma profiles for different discharge voltages.

The shape of the current-voltage curve $I_d(V_d)$ agrees well with experimental curves, and in particular with Fig.3 of Ref. 2 (the flow rate of Ref. 2 is smaller than in these simulations). For low discharge voltages $V_d < 150$V roughly, the discharge enters into the low-ionization regime, with a strong decrease in the propellant utilization, $\eta_u = I_{iC}/I_m$ (subscript C refers to the external boundary, Fig.1; $I_m = e\dot{m}_A/m_i$ represents the maximum ion current for a given mass flow, $I_m \simeq$ 3.5 A for $\dot{m}_A = 4.8$mg/s). For $V_d > 200V$, the plume ion current and the propellant utilization remain almost constant, $I_{iC} \sim 3A$ and $\eta_u \sim 80\%$. The increment of wall losses with V_d explains the deterioration of the current utilization $\eta_{cur} = I_{iC}/I_d$ and the thrust efficiency, $\eta = F^2/2\dot{m}_A I_d V_d$.

As V_d increases, the ionization rate increases (because of the higher electron temperature). However, the increment of the ion current lost in anode and lateral walls, $|I_{iA}|$ and I_W, makes the increment of plasma production totally useless. For $V_d \sim 450$V, the current recombined at the walls becomes equal to the plume ion current; similar relative losses have been reported from recent experiments.[13]

According to Ref. 10, the plume ion current (and η_u) is determined by the near-balance between volumetric ionization and wall recombination in the acceleration region. As a partial confirmation of this hypothesis, Fig. 8 shows that by augmenting artificially the ionization rate up to a 40%, the plume ion current I_{iC} increases, from 2.85A to 3.1A (which means an increment of $\sim 40\%$ in terms of $I_m - I_{iC}$).

A phenomenon that also influences the plasma production is the energy accommodation of ions

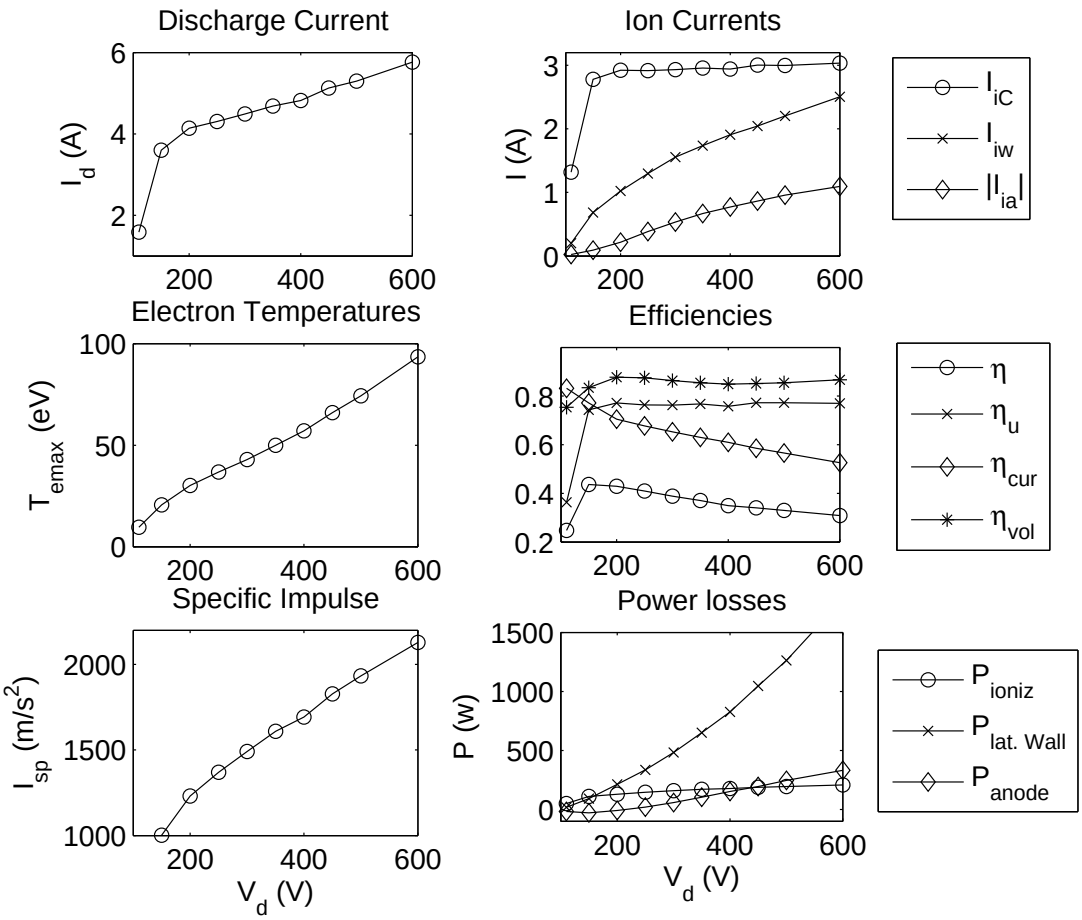

Figure 6. Evolution of thruster performances with the discharge voltage. Other parameters as in Fig. 2.

recombined at the walls. Higher energy accommodations mean higher neutral density and thus higher plasma production. Accommodation factors a_w of 60-80% are suggested in the Russian literature at the same time that $\eta_u > 90\%$ are reported.[13,14] The present code conciliates bad these two behaviors; for $a_w = 80\%$ we obtain $\eta_u \sim 80\%$ only. Propellant utilizations above 95% can be obtained with a_w near 100% (not shown here).

Therefore, unless near-total accommodation is justifiable, a revision of the ionization model is advisable. One could think on adding the electron (fluid) kinetic energy (due to the azimuthal drift mainly) to the internal energy in order to compute the ionization rate. The problem is that if the kinetic energy is of dominant order the diffusive model assumed for electrons becomes inconsistent. A second possibility to increase the ionization rate, which we are currently working on it, is the contribution of the high-energy, low-density beams of secondary electrons. A third possibility, partially related to the preceding one, comes from the suggestion that the ionization levels in a plasma discharge with micro-instabilities (generated by high current densities) can be quite different from those found by reaction rates based on local temperatures.[15]

The deterioration of performances for large V_d (Fig.6) is partially due to keep invariant the strength of the magnetic field, represented by B_{max}. As our macrosccopic models suggested already,[16,17] a consequence of that invariance is the increment of the ion back-current at the anode $|I_{iA}|$ with V_d increasing (Figs. 6 and 7); plasma density at the anode increases too (Fig. 7). Figure 9 illustrates how the ion current to the anode, $|I_{iA}|$, decreases by incrementing B_{max}. Then,

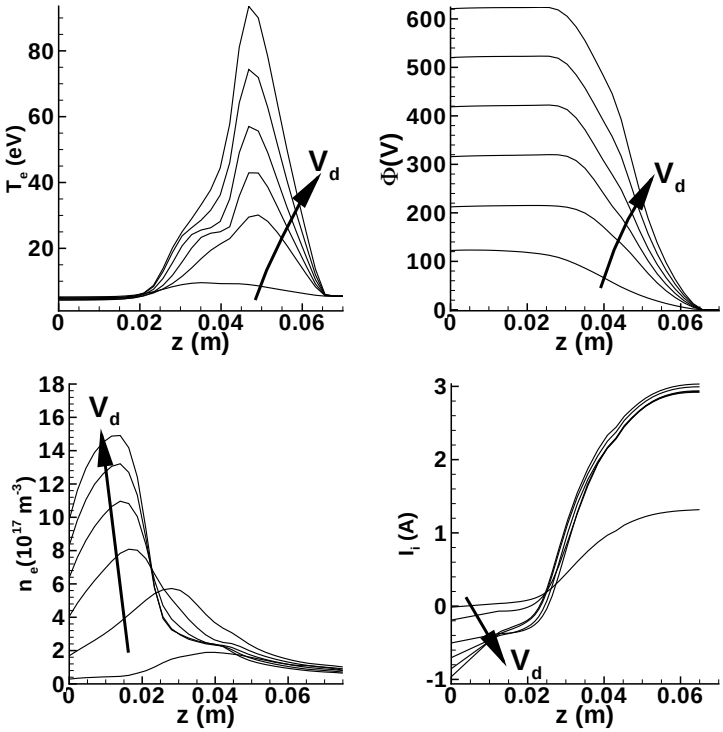

Figure 7. Evolution of plasma profiles with the discharge voltage, for V_d(in volts)= 110, 200, 300, 400, 500, 600. Profiles correspond to the channel median, $r = r_{med} = 49$mm except for the ion current I_i which is the real flux across surfaces $\lambda(r_{med}, z) =$ const.

the lower energy losses to anode reduce the total energy losses; this means a lower inwards electron current, $I_d - I_{iC}$, and therefore a lower discharge current I_d (notice that propellant utilization is governed by other aspects of the discharge).

The evolution, in Fig.6, of the maximum electron temperature with V_d follows $T_{e,max}/V_d \simeq 0.16$, which agrees reasonably well with Ref. 2. However, the experimental curve $T_{e,max}(V_d)$ presents a plateau for an intermediate range of discharge voltages, which is not found here. Also, the locations of the acceleration region and $T_{e,max}$ are almost invariant with V_d in the simulations, whereas experiments show an outward displacement of these locations with V_d.[2]

It is interesting to note that our quasi-2D macroscopic model[10,18] predicts both the plateau of the curve $T_{e,max}(V_d)$ and the displacements of the temperature peak and the acceleration region. According to that model (Barral et al.[19] obtain similar results), $T_{e,max}$ is located inside the thruster for low V_d, its position being decided by the relative contributions of Joule heating and ionization losses. As V_d increases, $T_{e,max}$ increases but the larger energy losses at the walls displace $T_{e,max}$ outwards. At a certain V_d, SEE approaches 100% near the thruster exit and electron energy losses become very high, limiting further increases of $T_{e,max}$ and creating the plateau of $T_{e,max}(V_d)$. For V_d high enough, $T_{e,max}$, already located outside the thruster, increases again.

The differences observed between the solutions of the macroscopic and hybrid codes require to be analyzed, mainly because the more ambitious HPHall-2 does not fit better the experiments. The modelling of physical phenomena is similar, but not identical, in the two codes. The treatment of radial dynamics in the macroscopic model could undervalue 2D effects. Also, neutrals are modelled crudely in the macroscopic code; the hybrid code shows a high sensitivity to injection conditions of neutrals (including those arising from recombination). Simulation conditions in the two codes are not identical too. For instance, the magnetic field was adjusted for each V_d in the macroscopic simulations, whereas it was kept constant here. Also, the macroscopic model is fully stationary

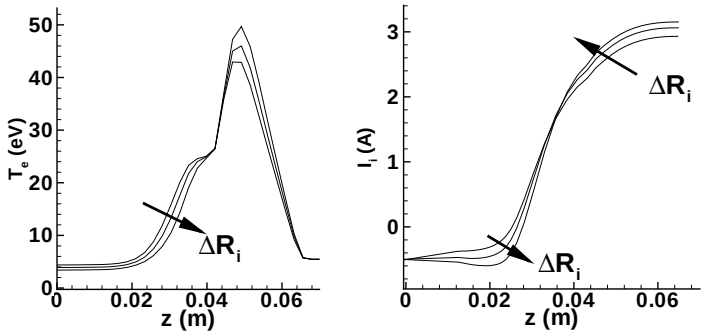

Figure 8. Influence of 'artificial' increments on the the ionization rate, $\Delta R_i = 0\%, 20\%, 40\%$. Same case than in Fig.2.

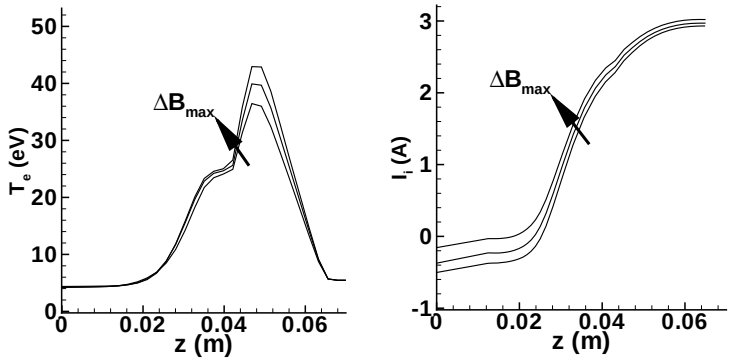

Figure 9. Influence of incrementing the magnetic field strength, for ΔB_{max}=0%, 20% and 40% with respect to case of Fig.2.

whereas the hybrid code simulations present a significant level of axial oscillations[3] (not shown in the time-averaged spatial maps, of course).

Figure 10 presents the only comparison between experimental plasma profiles and three simulations. Details are given in Table 1. Simulation 1 corresponds to the conditions assumed in all preceding simulations. Simulation 2 pretends to fit the temperature profile in the external plume. The increase of E_1^{eff} (energy for 100% SEE) in simulation 3 corresponds approximately to have decreased the thermalization fraction of the electron distribution function from $\sim 80\%$ to $\sim 50\%$. We observe a better fitting of the maximum plasma temperature, which confirms the diagnostic that energy deposition at the wall is too high when total thermalization is assumed. The implementation of the electron-wall model of Ref. 8 in the simulation code should provide a consistent, more-realistic model for the combined problems of partial thermalization and wall interaction on electrons. The differences with experiments on ion and discharge currents can be reduced by changing the parameter α_{ano} for Bohm diffusion. This will also affect somehow the profiles of the electric potential and the temperature in the acceleration region. The new cathode model presented in Ref. 5 will modify the external profiles too.

	T_{eC}	z_C	E_1^{eff}(eV)	I_{iC}(A)	I_d(A)
experiment				3.56	4.56
simulation 1	5	20	47	2.92	4.14
simulation 2	10	30	47	3.11	4.06
simulation 3	10	30	70	2.48	3.55

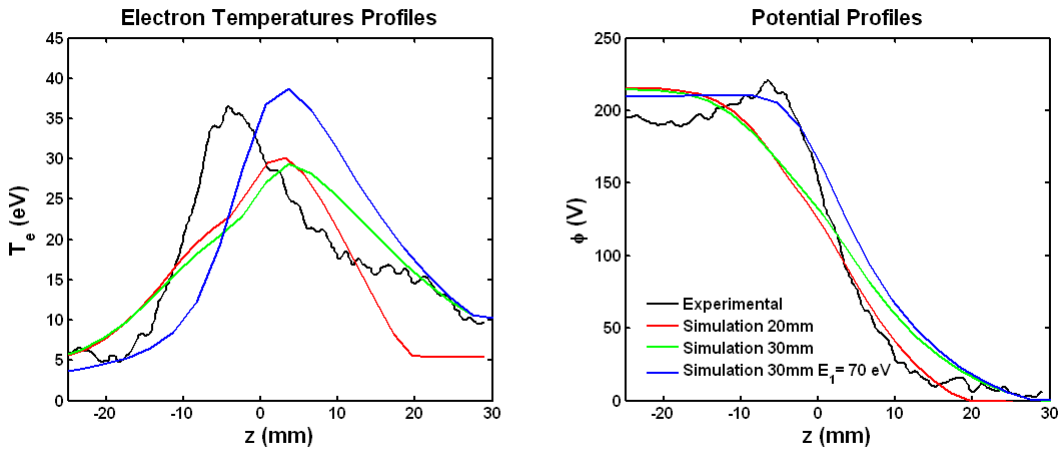

Figure 10. Comparison of experimental results for $V_d \sim 200$V with three simulation cases. Thruster exit is at $z = 0$.

III. Conclusions

The simulations made so far show a promising qualitative agreement with experiments in basic aspects of the plasma response but reveals also differences that suggest that improvements in the physical modelling are needed.

A methodic comparison between simulations and experimental results at different operation points must be undertaken yet. This will confirm the points of discrepancy, the probable causes, and possible solutions. This includes to continue testing the sensitivity of the simulations to small changes on the physical models implemented in the code.

One immediate improvement should be the modification of the wall-interaction subcode in order to account consistently for partial thermalization of the electron distribution function. The changes that a non-Maxwellian distribution function introduce in the quasineutral plasma model remain to be investigated.

A revision of the ionization processes and modelling seems necessary too.

Acknowledgments

Research at UPM was financed by the Ministerio de Ciencia y Tecnología of Spain (Project ESP-2004-03093) and by a grant from AFOSR. Work at PPPL was supported by grants from US DOE and AFOSR.

References

[1]Y. Raitses, D. Staack, L. Dorf, and N.J. Fisch. Experimental study of acceleration region in a 2kW Hall thruster. In *39th Joint Propulsion Conference, Huntsville, AL*, AIAA 2003-5153. American Institute of Aeronautics and Astronautics,Washington, DC, 2003.

[2]Y. Raitses, D. Staack, A. Smirnov, and N. J. Fisch. Space charge saturated sheath regime and electron temperature saturation in Hall thrusters . *Physics of Plasmas*, 12:073507, 2005.

[3]F.I. Parra, E. Ahedo, M. Fife, and M. Martínez-Sánchez. A two-dimensional hybrid model of the Hall thruster discharge . *Journal of Applied Physics (to appear in July 2006)*.

[4]D. Escobar, E. Ahedo, and F. I. Parra. On conditions at the sheath boundaries of a quasineutral code for Hall thrusters. In *Proc. 29th International Electric Propulsion Conference, Princeton, USA*, IEPC-2005-041. Electric Rocket Propulsion Society, Fairview Park, OH, 2005.

[5]A. Antón and E. Ahedo. New contour algorithms for a Hall thruster hybrid code. In *42th Joint Propulsion*

Conference, Sacramento, CA, AIAA-2006-4834. American Institute of Aeronautics and Astronautics,Washington, DC, 2006.

[6]A. Dunaevsky, Y. Raitses, and N. J. Fisch. Secondary electron emission from dielectric materials of a Hall thruster with segmented electrodes . *Physics of Plasmas*, 10(6):2574 – 2577, 2003.

[7]E. Ahedo and F.I. Parra. Partial trapping of secondary electron emission in a Hall thruster plasma. *Physics of Plasmas*, 12(7):073503, 2005.

[8]E. Ahedo. Effects of electron secondary emission and partial thermalization on a Hall thruster plasma. In *42th Joint Propulsion Conference, Sacramento, CA*, AIAA-2006-4328. American Institute of Aeronautics and Astronautics,Washington, DC, 2006.

[9]G.S. Janes and R.S. Lowder. Anomalous electron diffusion and ion acceleration in a low-density plasma . *Physics of Fluids*, 9(6):1115–1123, 1966.

[10]E. Ahedo, J.M. Gallardo, and M. Martínez-Sánchez. Effects of the radial-plasma wall interaction on the axial Hall thruster discharge. *Physics of Plasmas*, 10(8):3397–3409, 2003.

[11]F.I. Parra and E. Ahedo. Fulfillment of the Bohm condition on the HPHall fluid-PIC code. In *Proc. 40th Joint Propulsion Conference, Fort Lauderdale, FL*, AIAA 2004-3955. American Institute of Aeronautics and Astronautics,Washington, DC, 2004.

[12]L. Dorf, Y. Raitses, and N. J. Fisch. Effect of magnetic field profile on the anode fall in a Hall-effect thruster discharge . *Physics of Plasmas*, 13.

[13]V. Kim, V.I. Kozlov, A.I. Skrylnikov, L.N. Umnitsin, V.V. Svotina, A. Bouchoule, and M. Prioul. Investigation of the Local Plasma Parameter Distributions in the SPT Accelerating Channel Under Increased Discharge Voltages. In *29th International Electric Propulsion Conference, Princeton, USA*, IEPC-2005-004. Electric Rocket Propulsion Society, Fairview Park, OH, 2005.

[14]A.I Morozov and V.V. Savelyev. *Reviews of Plasma Physics*, volume 21, chapter 2. Kluwer Academic, New York, 2000.

[15]P.J. Turchi. *Space propulsion analysis and design*, chapter Electric rocket propulsion systems. Kluwer and Microcosm, 1995.

[16]E. Ahedo, P. Martínez-Cerezo, and M. Martínez-Sánchez. 1-D performance analysis of a Hall thruster. In *SP-465: 3rd Spacecraft Propulsion Conference, Cannes (France)*, pages 323–330, Noordwijk, The Netherlands, 2000. European Space Agency.

[17]E. Ahedo and J.Rus. Vanishing of the negative anode sheath in a Hall thruster. *Journal of Applied Physics*, 98:043306, 2005.

[18]E. Ahedo and D. Escobar. Influence of design and operation parameters on Hall thruster performances. *Journal of Applied Physics*, 96(2):983–992, 2004.

[19]S. Barral, K. Makowski, Z. Peradzynski, N. Gascon, and M. Dudeck. Wall material effects in stationary plasma thrusters. II. Near-wall and in-wall conductivity . *Phys. Plasmas*, 10(10):4137 – 4152, 2003.